Journal of Alloys and Compounds 509 (2011) 8922–8926

Contents lists available at ScienceDirect

Journal of Alloys and Compounds

journal homepage: www.elsevier.com/locate/jallcom

Structural, optical and electrical properties of N-doped ZnO thin films prepared by thermal oxidation of pulsed filtered cathodic vacuum arc deposited Zn_xN_y films

N.H. Erdogan[a], K. Kara[a], H. Ozdamar[a], H. Kavak[a,*], R. Esen[a], H. Karaagac[b]

[a] Physics Department, Cukurova University, 01330 Adana, Turkey
[b] Physics Department, Middle East Technical University, 06531 Ankara, Turkey

ARTICLE INFO

Article history:
Received 8 February 2011
Received in revised form 7 June 2011
Accepted 13 June 2011
Available online 22 June 2011

PACS:
73.6.Ga
78.55.Cr
78.66.Hf
79.60.–I

Keywords:
Thin films
Semiconductors
Crystal structure
Oxidation
X-ray diffraction

ABSTRACT

In this study, N-doped ZnO thin films were fabricated by oxidation of Zn_xN_y films. The Zn_xN_y thin films were deposited on glass substrates by pulsed filtered cathodic vacuum arc deposition (PFCVAD) using metallic zinc wire (99.999%) as a cathode target in pure nitrogen plasma. The influence of oxidation temperature, on the electrical, structural and optical properties of N-doped ZnO films was investigated. P-type conduction was achieved for the N-doped ZnO obtained at 450 °C by oxidation of Zn_xN_y, with a resistivity of 16.1 Ω cm, hole concentration of 2.03×10^{16} cm^{-3} and Hall mobility of 19 cm^2/V s. X-ray photoelectron spectroscopy (XPS) analysis confirmed the incorporation of N into the ZnO films. X-ray diffraction (XRD) pattern showed that the films as-deposited and oxidized at 350 °C were amorphous. However, the oxidized films in air atmosphere at 450–550 °C were polycrystalline without preferential orientation. In room temperature photoluminescence (PL) spectra, an ultraviolet (UV) peak was seen for all the samples. In addition, a broad deep level emission was observed.

© 2011 Elsevier B.V. All rights reserved.

1. Introduction

ZnO is a direct wide band-gap ($E_g \sim 3.37$ eV) semiconducting material, with a large exciton binding energy of 60 meV and possess good transparency in the visible wavelength [1,2]. These properties make the ZnO an important semiconductor for various applications in optoelectronic devices such as UV light-emitting diodes, laser diodes and photodetectors [1,3]. To reach such goals, the fabrication of stable and reproducible n and p-type ZnO with excellent electrical and optical properties are very important [1,4,5]. n-type ZnO is easily available with high quality by Al [6], Ga [7] or In [8] doping. However, the fabrication of p-type ZnO is difficult due to the low solubility of the acceptor dopant, deep acceptor level and self-compensation effect involving native defects such as oxygen vacancies (V_o) and zinc interstitials (Zn_i), etc. [2,9,10].

In recent years, many works have been attempted to produce p-type ZnO films using various dopants. It has been suggested that p-type doping in ZnO can be achieved through substituting either group I elements, such as Na [11], K [12] or Li [13] with Zn or group V elements, such as N [10], P [14], As [5] or Sb [3] for oxygen. Furthermore, Li–N [9] and Al–N [2] co-doped ZnO films have also been studied to produce p-type ZnO.

ZnO thin films doped with group I or group V elements usually exhibit low hole mobility and low hole concentration [4,10,11,15]. It is well known that nitrogen is the most promising candidate due to small ionic size and low energy level of substitution (N_O) [10,15]. However, there have been only very limited reports on the N-doped p-type ZnO mainly due to the low doping efficiency and instability of substitutional nitrogen molecule (N_2) in the host ZnO. One of the reasons for that behavior is the deactivation of N_O to form compensatory nitrogen molecule (N_2) in the host ZnO, in high temperature annealing process, which is usually needed to activate acceptor in N-doped ZnO. However, the formation of N_2 molecule and key step to prevent its formation are still uncertain [16,17].

Many thin film preparation techniques have been applied in the synthesis of p-type ZnO films including a molecular beam epitaxy [18], metal organic chemical vapor deposition [4], magnetron sputtering [10], pulsed laser deposition [19], sol gel processing [2] and so on. It is known that good quality dense carbon coatings are produced by filtered cathodic vacuum arc (FCVA) technique. The

* Corresponding author. Tel.: +90 322 3386801; fax: +90 322 3386070.
E-mail address: hkavak@cu.edu.tr (H. Kavak).

0925-8388/$ – see front matter © 2011 Elsevier B.V. All rights reserved.
doi:10.1016/j.jallcom.2011.06.048

impact energy of the depositing ions at the growth surface can be readily controlled using electric fields due to the 100% ionization of the cathode materials in the plasma. Their high-energy plasma plume ionizes most background gases. These features make the FCVA an ideal source for the production of metal oxides and nitrides [20]. In this study, we realized N-doped ZnO thin films by thermal oxidation of Zn_xN_y which was deposited by PFCVAD. The structural, electrical and optical properties of the thin films were characterized as a function of oxidation temperature.

2. Experimental procedures

Zinc nitride (Zn_xN_y) thin films were deposited on glass substrates (Corning 2947) through PFCVAD system. Metallic zinc (1 mm in diameter and purity 99.999%) which was held in an alumina ceramic tube was employed as a cathode target. The deposition chamber was evacuated using a primary and a turbo molecular pump. The details of the deposition system were published in earlier studies [21]. In this study, the substrate temperature was kept at 25 °C. The glass substrates were cleaned in an ultrasonic bath with acetone for 20 min at room temperature then washed using deionized water and finally dried by nitrogen blowing. The base pressure of the deposition chamber was $\sim 2.6 \times 10^{-6}$ Torr and the working pressure was 8.5×10^{-4} Torr. High purity (99.999% pure) nitrogen, which is produced by nitrogen generator were introduced into the chamber and controlled by multi gas controller. During the deposition, the nitrogen gas flow was fixed at 3.60 standard cubic centimeters per minute. In the course of the deposition process, trigger voltage and arc voltage were set to 20 kV and 580 V, respectively. All the films were deposited for 700 pulses and the thicknesses of the films which were evaluated from the transmittance spectra according to the interference theory were about 200 nm. After deposition, the films were oxidized at different temperatures for 1 h intervals in air.

The structural properties of the films were examined by XRD using a Rigaku Miniflex system with Cu Kα radiation (λ = 1.54059 Å). XPS spectra was obtained using a UNISPECS ESCA system equipped with a Mg Kα radiation source of energy value of 1253.6 eV in a high vacuum system with a base pressure of about 10^{-7} Pa. The optical properties of the films were investigated by a double beam computer controlled spectrophotometer (Perkin Elmer Lambda 2S) in the UV/VIS/NIR regions. The optical transmittance was recorded in the wavelength range of 300–1100 nm with 1 nm precision. The electrical properties of the films (resistivity, type of the conductivity, carrier concentration and mobility) were determined by the Hall-effect measurement system (HMS-3000), using the four-probe Van der Pauw technique. HMS-3000 system was also employed to check the linearity of the contacts. All the measurements were carried out at room temperature. In order to investigate the luminescence properties of the samples, PL measurement was performed at room temperature using a He–Cd laser (325 nm, 30 mW) as the excitation source.

3. Results and discussion

3.1. X-ray diffraction

XRD patterns of the as-deposited Zn_xN_y film and N-doped ZnO films obtained by oxidation of Zn_xN_y films between 350 and 550 °C are shown in Fig. 1. XRD patterns of the as-deposited and oxidized (1 h at 350 °C) samples did not display any well-defined peaks suggesting that they were amorphous in nature. With the increase of oxidation temperature from 350 to 550 °C, the diffraction peaks were observed at $2\theta = 32.49°$, 35.08°, 36.91°, 57.20° and were attributed to (1 0 0), (0 0 2), (1 0 1) and (1 1 0) planes of the hexagonal ZnO structure, respectively. The XRD patterns indicate that N-doped ZnO films obtained after oxidation at 450 and 550 °C possessed a polycrystalline hexagonal wurtzite structure without preferential orientation. When the oxidation temperature was increased from 450 to 550 °C, a small decrease of the intensity of the diffraction peak of the ZnO (1 0 0) was seen, while the intensity of diffraction peak of the ZnO (1 1 0) increased. On the other hand, when the oxidation temperature was 450 °C, the diffraction peak of the ZnO (1 0 1) was sharp and intense but, with a further increase of oxidation temperature to 550 °C, the intensity of this peak clearly decreased and the diffraction peak of the ZnO (0 0 2) became sharper and more intense. The grain size can be evaluated using Scherrer's formula.

$$D = \frac{0.9\lambda}{\beta \cos\ \theta} \tag{1}$$

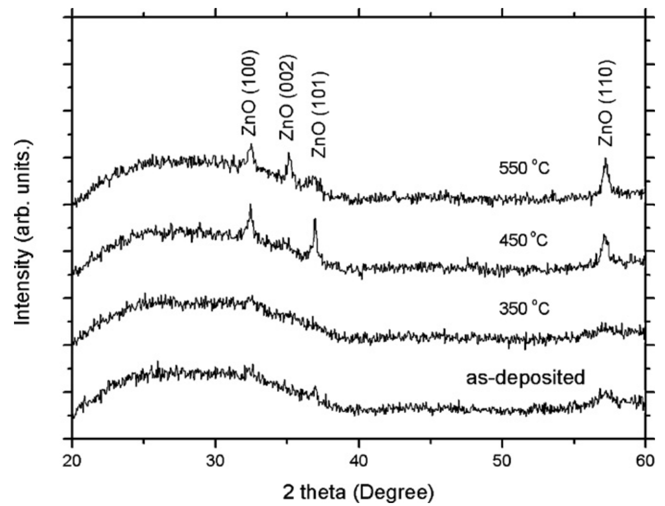

Fig. 1. The XRD spectra of the as-deposited Zn_xN_y film and N-doped ZnO films obtained by oxidation of Zn_xN_y films between 350 and 550 °C.

where D is the grain size, λ is the wavelength of the X-ray radiation used, β is the full width at half maximum (FWHM) of the diffraction peak, and θ is the Bragg diffraction angle of the XRD peak [22]. The grain size of the samples obtained by oxidation of Zn_xN_y at various temperatures ranged between 9.75 and 36.37 nm. The interplanar distance (d_{hkl}) as calculated from XRD for (1 0 0), (0 0 2), (1 0 1), and (1 1 0) peaks were 0.27553, 0.25576, 0.24349 and 0.16102 nm, which were smaller than the corresponding bulk values of 0.282, 0.260, 0.248 and 0.163 nm (JCPDS card No. 80-0075) [23]. The films with values of lattice parameters greater than the theoretical value have a positive or extensive strain in them whereas those with lower values have a negative or compressive strain [24]. Thus the lower values of lattice constant than those of bulk values were indicative of compression stress, which was caused by the formation of point defects that can be proved by PL measurement [25]. Besides, since the diffraction peak position for each orientation did not change greatly with increasing oxidation temperature, the lattice constant of ZnO was almost independent of the oxidation temperature.

3.2. X-ray photoelectron spectroscopy

XPS measurement was performed to analyze the chemical bonding states of Zn, O and N in the film obtained after oxidation at 450 °C. To avoid the adventitious contaminants, the surface of the sample was sputtered for 2 min by Argon (Ar^+) ions with energy of 2000 eV prior to the XPS measurements. Binding energies were corrected for charging effect with reference to the adventitious carbon 1s peak at 284.6 eV. C peaks came from the surface adsorption of CO_2. After sputtering with Ar ions, a noticeable reduction related to C1s peak intensity was observed, suggesting surface adsorption of CO_2. The XPS spectra of N 1s core level were deconvolved into three components using XPSPeak41 software and the profile of each peak was taken as an 80% Lorentzian and 20% Gaussian mixed function. Fig. 2 shows the XPS spectra of N 1s core level. Three peaks at the binding energies of 396.5, 399.4 and 405 eV were detected in the N 1s region. The lower peak centered at 396.5 eV was attributed to typical Zn–N bonds [4]. According to our XPS spectra, a small amount of C element still appeared on the surface of the sample after sputtering processes. Thus, the N 1s peak at around 399.33 eV could be ascribed to C–N bound [25]. The higher peak centered around 405 eV was associated with terminally bonded γ-N_2 states [26].

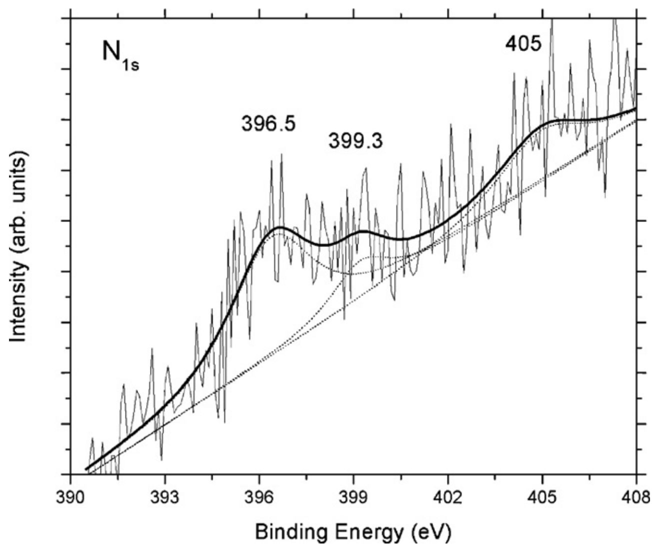

Fig. 2. XPS spectra of N 1s core levels for the sample obtained after thermal oxidation at 450 °C.

Fig. 3 shows the XPS spectra of O 1s core level. The XPS spectra of O 1s core level were deconvolved into two components located at 530 and 531.8 eV, the profile of each peak was taken as a 20% Lorentzian and 80% Gaussian mixed function. The peak centered at 530 eV was related to Zn–O bonds. The higher energy peak at 531.8 eV could be related to the presence of water or OH bonds [27].

Fig. 4 shows the core level peaks of Zn 2p. The binding energy of Zn $2p_{3/2}$ was located at 1021.2 eV, which is the value of Zn in ZnO.

3.3. Hall-effect

To investigate the doping mechanism and influence of oxidation temperature on the electrical properties of N-doped ZnO films, Hall-effect measurements were carried out as a function of oxidation temperature. The ohmic contacts were made by soldering indium metal to the four corners of the square shaped sample. Excellent linearity was observed from the current voltage curves for the contacts on the sample, indicating good ohmic contacts between N doped ZnO and In. The magnitude of the magnetic field was 0.54 T,

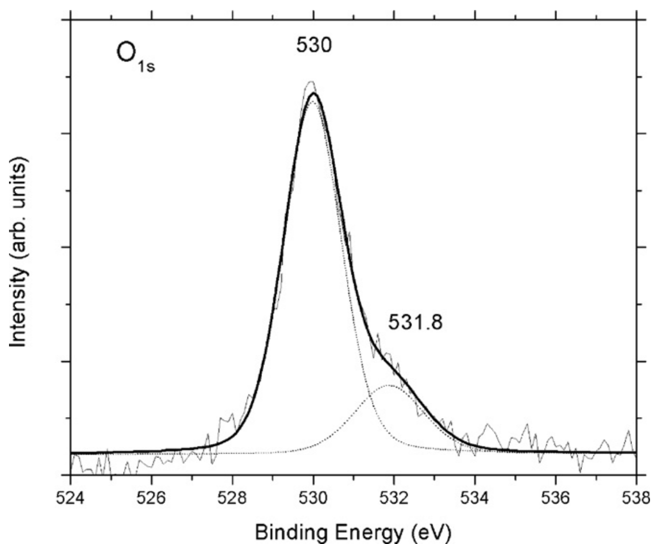

Fig. 3. XPS spectra of O 1s core levels for the sample obtained after thermal oxidation at 450 °C.

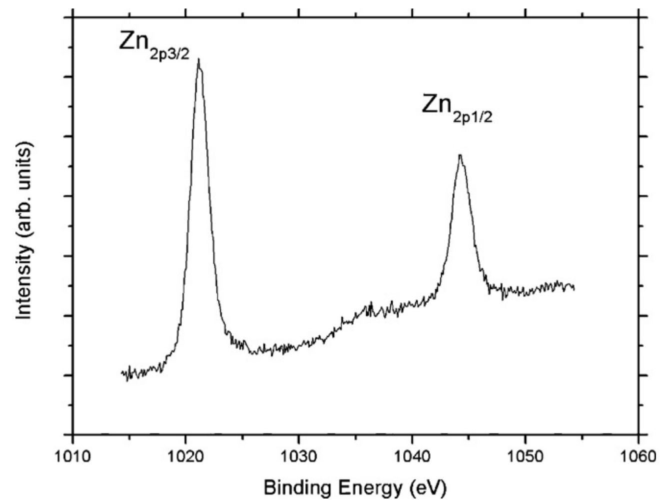

Fig. 4. XPS spectra of Zn 2p core levels for the sample obtained after thermal oxidation at 450 °C.

and typical values of the currents were chosen as 1 nA and 0.5 μA for the films obtained by oxidation of Zn_xN_y films at 350 °C and 450–550 °C, respectively. The Hall measurements were repeated several times for each sample to ensure reliability of the results. The results of the room temperature Hall measurements are listed in Table 1.

The film oxidized at 350 °C showed an ambiguous conduction type. However, with the increase of oxidation temperature from 350 to 450 °C, more N acceptors began to be activated and as a result more holes were produced, which led to an increase of hole concentration, so the film obtained after oxidation at 450 °C showed definite p-type conduction [28,29]. However, with a further increase of oxidation temperature to 550 °C, the conduction type was changed from p-type to n-type. This result was attributed to a decrease of N concentration in ZnO with increasing oxidation temperature as reported previously [28–30]. The optimized result was realized for the film obtained after oxidation at 450 °C with a resistivity of 16.1 Ω cm, a hole concentration and Hall mobility of 2.03×10^{16} cm^{-3} and 19 cm^2/V s, respectively.

The reproducibility and stability of the p-type ZnO:N film was also investigated. Two additional Zn_xN_y films were obtained under the same condition and oxidized at 450 °C. These two films obtained after oxidation at 450 °C exhibited a resistivity of 21.6–35.9 Ω cm and hole concentration of 2.11×10^{16}–5.53×10^{16} cm^{-3} and Hall mobility of 13.6–3.1 cm^2/V s. Six month later, all the films obtained after oxidation at 450 °C exhibited a resistivity of 90.1–28.7 Ω cm and hole concentration of 6.37×10^{15}–1.03×10^{16} cm^{-3} and Hall mobility of 10.8–21.1 cm^2/V s. However, in about 1 year, all the films exhibited higher resistivity (up to 200 Ω cm) and lower carrier concentration (10^{14}–10^{15} cm^{-3}). Besides, all the film obtained after oxidation at 450 °C showed ambiguous conduction type after 1 year. Thus, the film obtained after oxidation at 450 °C was reproducible but the stability of p-type behavior in the films was still doubtful.

Table 1
The results of Hall effect measurements.

Oxidation temperature (°C)	Carrier concentration (cm^{-3})	Mobility (cm^2/V s)	Resistivity (Ω cm)	Type
350	1.28×10^{12}	2.67×10^{1}	1.82×10^{5}	n or p
450	2.03×10^{16}	1.90×10^{1}	1.61×10^{1}	p
550	6.47×10^{16}	1.67×10^{0}	5.74×10^{1}	n

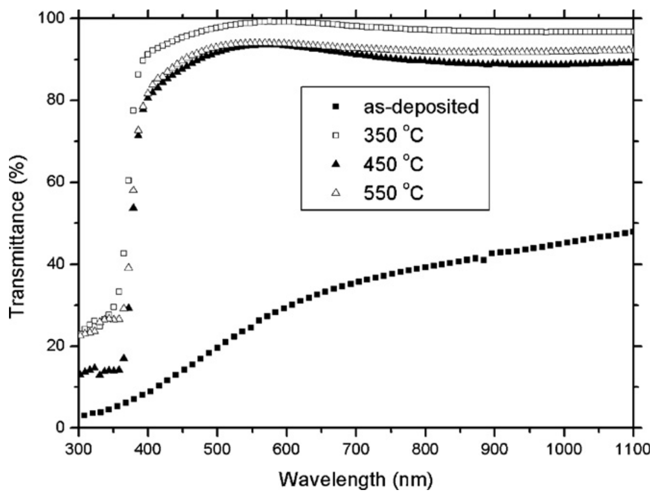

Fig. 5. The optical transmittance of the as-deposited Zn_xN_y film and N-doped ZnO films obtained at different oxidation temperatures.

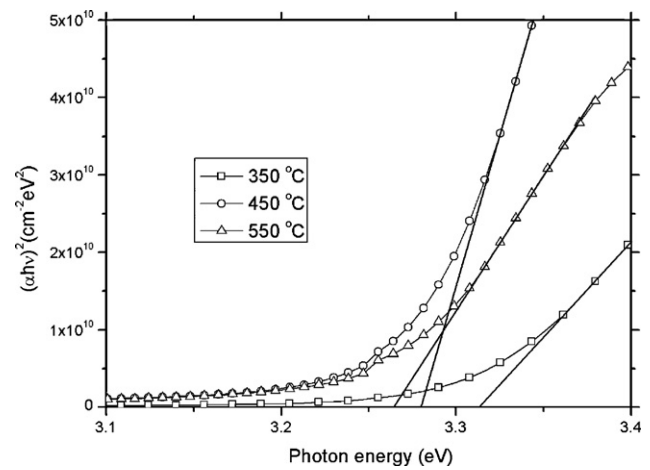

Fig. 6. $(\alpha h\nu)^2$ vs. $h\nu$ plots of N-doped ZnO films obtained by oxidation of Zn_xN_y films between 350 and 550 °C.

3.4. Optical properties

The optical transmittance spectra recorded in the wavelength ranging from 300 to 1100 nm for the as-deposited Zn_xN_y film and N-doped ZnO films which were obtained by oxidation of Zn_xN_y between 350 and 550 °C are shown in Fig. 5. The transmittance of the as-deposited Zn_xN_y was very low due to excess of Zn in the structure of the film [31]. After oxidation, all the samples became more transparent and their transmittance in the visible range was above 85%. When the oxidation temperature was increased from 350 to 450 °C, the optical transmittance decreased. On the other hand, with a further increase of oxidation temperature to 550 °C, the optical transmittance increased again. In addition, very sharp near UV absorption edges were observed at 374.28, 379.90 and 378.04 nm for all the samples after oxidation between 350 and 550 °C, indicating that the films had pure ZnO phase and very strong UV absorption properties.

As a direct band gap semiconductor, ZnO film has an absorption coefficient (α) obeying the following relation for high photon energies ($h\nu$)

$$a(h\nu) = A(h\nu - E_g)^{1/2} \quad (2)$$

where E_g is the optical band gap of thin film, and A is a constant [32,33]. Near the absorption edge, α can be expressed as

$$a = -\frac{\mathrm{Ln}(T)}{d} \quad (3)$$

where d is the film thickness [34]. The plot of $(\alpha h\nu)^2$ vs. the photon energy ($h\nu$) in the absorption region of the samples is shown in Fig. 6. The optical band gap energy E_g can be estimated from the obtained absorption spectrum by extrapolating the linear portion of $(\alpha h\nu)^2$ vs. $h\nu$ to $\alpha = 0$ [32,33]. The optical band gap energies were determined to be about 3.313, 3.280 and 3.264 eV for the N-doped ZnO films obtained after oxidation at 350, 450, and 550 °C, respectively. The optical energy band gap was decreased with the increase of oxidation temperature from 350 to 550 °C. The changes in the reported values in band gap of the ZnO can arise from the presence of growth stresses, thermal expansion mismatch stresses and dopants [34]. The Pauling theory says that a large difference in the electronegativity between two elements forming the single bond leads to higher ionicity in the bond. The electronegativity of Zn is 1.6 eV, and the electronegativity of O (3.5) is larger than that of N (3.0), so the Zn–O band has larger ionicity than the Zn–N band. From the Hall-effect measurements, we know that more N-acceptors were activated with the increase of oxidation temperature from 350 to 450 °C, so the decrease in E_g was probably attributed to the decrease in ionicity and formation of Zn–N bands in the films [35]. On the other hand, we know that N concentration in ZnO decreased with a further increase of oxidation temperature to 550 °C. Thus, the out diffusion of N impurities from the film created vacancies and other defects. Therefore, a further decrease of E_g was also observed, when the oxidation temperature was 550 °C [34].

3.5. Photoluminescence

Room temperature photoluminescence measurements for nitrogen-doped ZnO films obtained at different oxidation temperatures are shown in Fig. 7. The spectra were dominated by 3.327 eV and 3.294 eV emissions for the N-doped ZnO after oxidation at 350 °C and 450–550 °C, respectively. The origin of the near-band edge (NBE) UV emissions at 3.327 and 3.294 eV were from the recombination of free excitons [25,30,36]. The luminescence probably consisted of the overlap of free excitons and bound excitons [28]. In room temperature PL spectra, no acceptor-related emissions, such as donor–acceptor pair transitions (D^oA^o) or neutral-acceptor-bound exciton emission (A^oX) were observed due to the thermal effect quenching [30]. Also a broad deep level emission has been observed between 1.8 and 2.7 eV. The blue-green band emission and orange-red band emission for the N-doped

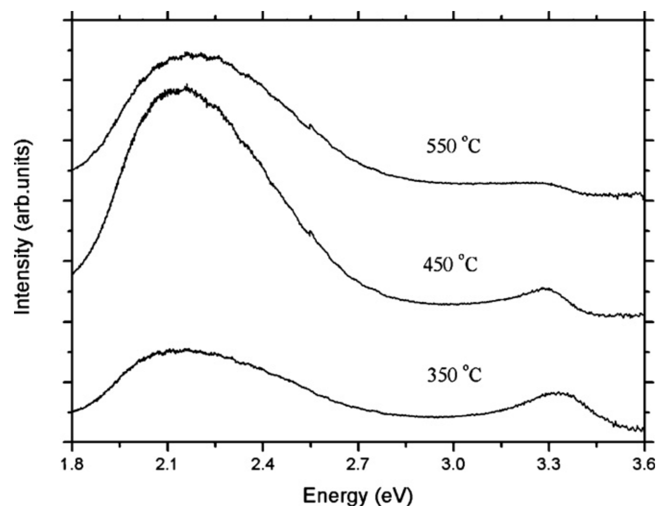

Fig. 7. The photoluminescence spectra measured at room temperature for N-doped ZnO films obtained by oxidation of Zn_xN_y films between 350 and 550 °C.

ZnO were attributed to deep acceptor levels. The broad blue-green band emission from the ZnO is generally explained as the radiative recombination of a photo generated hole with the electron at the singly ionized intrinsic oxygen vacancies [34,37,38]. Orange band emission and red band emission are usually attributed to Zn_i, or single ionized O interstitial (O_i^-) or Zn_i-related defects (or called Zn_i complex) [20,39]. Thus, the defect-related emission in the visible region could be ascribed to oxygen vacancies, zinc interstitials, etc. With the increase of oxidation temperature from 350 to 550 °C, the intensity of the peak in the visible region increased, indicating the increase of point defects.

4. Conclusions

The Zn_xN_y thin films on glass substrates were deposited by pulsed filtered cathodic vacuum arc using metallic zinc as the cathode target in nitrogen plasma and oxidized between 350 and 550 °C in air atmosphere. The XRD pattern shows that the as-deposited and oxidized (at 350 °C) Zn_xN_y films were amorphous. The Zn_xN_y films oxidized in air at 450–550 °C were polycrystalline without any preferential orientation. The films after oxidation at 350 °C showed ambiguous conduction type, while the film after oxidation at 450 °C showed definite p-type conductivity. On the other hand, when the oxidation temperature reached to 550 °C, the conduction type of the film converted to n-type. The XPS spectra showed a typical N 1s peak at 396.5 eV, which is usually attributed to N atoms on O sites (N_O) to act as acceptors. The UV–visible spectra show that the transmittance of as-deposited Zn_xN_y was very low and after oxidation, all the samples became more transparent and their transmittance in the visible range was above 85%. Also the UV absorption edge at 374–378 nm was observed for all the oxidized samples. In room temperature PL spectra, an UV emission and a broadband visible emission were observed for all the films.

Acknowledgments

This work is supported by the Research Found of Cukurova University and the Scientific and Technological Research Council of Turkey (Grant No.: 106T613).

References

[1] Y.C. Huang, L.W. Weng, W.Y. Uen, S.M. Lan, Z.Y. Li, S.M. Liao, T.Y. Lin, T.N. Yang, J. Alloys Compd. 509 (2011) 1980–1983.
[2] I.Y. Bu, J. Alloys Compd. 509 (2011) 2874–2878.
[3] T. Yang, B. Yao, T.T. Zhao, G.Z. Xing, H. Wang, H.L. Pan, R. Deng, Y.R. Sui, L.L. Gao, H.Z. Wang, T. Wu, D.Z. Shen, J. Alloys Compd. 509 (2011) 5426–5430.
[4] Q. Li, J. Bian, J. Sun, H. Liang, C. Zou, Y. Sun, Y. Luo, Appl. Surf. Sci. 257 (2010) 1634–1637.
[5] A. Kumar, M. Kumar, B.P. Singh, Appl. Surf. Sci. 256 (2010) 7200–7203.
[6] Z. Zhang, C. Bao, W. Yao, S. Ma, L. Zhang, S. Hou, Superlattices Microstruct. 49 (2011) 644–653.
[7] X. Bie, J. Lu, Y. Wang, L. Gong, Q. Ma, Z. Ye, Appl. Surf. Sci. 257 (2011) 6125–6128.
[8] Y.S. Rim, H.J. Kim, K.H. Kim, Thin Solid Films 518 (2010) 6223–6227.
[9] D. Zhang, J. Zhang, Z. Guo, X. Miao, J. Alloys Compd. 509 (2011) 5962–5968.
[10] T.L. Dan, W. Bing, Z. Yue, J. Alloys Compd. 509 (2011) 384–386.
[11] S.S. Lin, J.G. Lu, Z.Z. Ye, H.P. He, X.Q. Gu, L.X. Chen, J.Y. Huang, B.H. Zhao, Solid State Commun. 148 (2008) 25–28.
[12] L. Xu, F. Gu, J. Su, Y. Chen, X. Li, X. Wang, J. Alloys Compd. 509 (2011) 2942–2947.
[13] B. Wang, L. Tang, J. Qi, H. Du, Z. Zhang, J. Alloys Compd. 503 (2010) 436–438.
[14] S.C. Su, X.D. Yang, C.D. Hu, Physica B 406 (2011) 1533–1535.
[15] L.C. Chao, Y.R. Shih, Y.K. Li, J.W. Chen, J.D. Wu, C.H. Ho, Appl. Surf. Sci. 256 (2010) 4153–4156.
[16] J. Gao, R. Qin, G. Luo, J. Lu, Y.L. Wang, H. Ye, Z. Liao, Q. Zhao, D. Yu, Phys. Lett. A 374 (2010) 3546–3550.
[17] J. Karamdel, C.F. Dee, B.Y. Majlis, Appl. Surf. Sci. 256 (2010) 6164–6167.
[18] S.H. Park, J.H. Chang, T. Minegishi, J.S. Park, I.H. Im, M. Ito, T. Taishi, S.K. Hong, D.C. Oh, M.W. Cho, T. Yao, J. Cryst. Growth 311 (2009) 2167–2171.
[19] Z. Zhao, L. Hu, H. Zhang, J. Sun, J. Bian, J. Zhao, Appl. Surf. Sci. 257 (2011) 5121–5124.
[20] X.L. Xu, S.P. Lau, J.S. Chen, G.Y. Chen, B.K. Tay, J. Cryst. Growth 223 (2001) 201–205.
[21] E. Senadim, H. Kavak, R. Esen, J. Phys.: Condens. Matter 18 (2006) 6391–6400.
[22] Y. Zhang, B. Lin, Z. Fu, C. Liu, W. Han, Opt. Mater. 28 (2006) 1192–1196.
[23] P. Kumbhakar, D. Singh, S. Tiwary, A.K. Mitra, Chalcogenide Lett. 5 (2008) 387–394.
[24] R. Vinodkumar, K.J. Lethy, D. Beena, M. Satyanarayana, R.S. Jayasree, V. Ganesan, V.U. Nayar, V.P. Mahadevan Pillai, Sol. Energy Mater. Sol. Cells 93 (2009) 74–78.
[25] Y. Zhu, S. Lin, Y. Zhang, Z. Ye, Y. Lu, J. Lu, B. Zhao, Appl. Surf. Sci. 255 (2009) 6201–6204.
[26] W.T. Wu, L. Shi, Q. Zhu, Y. Wang, G. Xu, W. Pang, Mater. Lett. 61 (2007) 4752–4755.
[27] A. Toumiat, S. Achour, A. Harabi, N. Tabet, M. Boumaour, M. Maallemi, Nanotechnology 17 (2006) 658–663.
[28] B.S. Li, Y.C. Liu, Z.Z. Zhi, D.Z. Shen, Y.M. Lu, J.Y. Zhang, X.W. Fan, J. Mater. Res. 18 (2003) 8–13.
[29] C. Wang, Z. Ji, K. Liu, Y. Xiang, Z. Ye, J. Cryst. Growth 259 (2003) 279–281.
[30] Y.J. Zheng, Z.Z. Ye, W.Z. Xu, B. Liu, Y. Che, L.P. Zhu, B.H. Zhao, Mater. Lett. 61 (2007) 41–44.
[31] V. Kambilafka, P. Voulgaropoulou, S. Dounis, E. Iliopoulos, M. Androulidaki, V. Saly, M. Ruzinsky, E. Aperathitis, Superlattices Microstruct. 42 (2007) 55–61.
[32] Z. Yan, Z.T. Song, W.L. Liu, Q. Wan, F.M. Zhang, S.L. Feng, Thin Solid Films 492 (2005) 203–206.
[33] Y. Miao, Z. Ye, W. Xu, F. Chen, X. Zhou, B. Zhao, L. Zhu, J. Lu, Appl. Surf. Sci. 252 (2006) 7953–7956.
[34] X.C. Wang, W.M. Bi, S. Dong, X.M. Chen, B.H. Yang, J. Alloys Compd. 478 (2009) 507–512.
[35] J. Lu, Z. Ye, L. Wang, J. Huang, B. Zhao, Mater. Sci. Semicond. Process. 5 (2003) 491–496.
[36] J.M. Erie, Y. Li, M. Ivill, H.S. Kim, S.J. Pearton, B. Gila, D.P. Norton, F. Ren, Appl. Surf. Sci. 254 (2008) 5941–5945.
[37] T. Zaidi, W.E. Fenwick, A. Melton, N. Li, S. Gupta, H. Yu, A. Ougazzaden, L. Ferguson, J. Cryst. Growth 310 (2008) 5011–5015.
[38] M. Kumar, B.T. Lee, Appl. Surf. Sci. 254 (2008) 6446–6449.
[39] B. Yao, L.X. Guan, G.Z. Xing, Z.Z. Zhang, B.H. Li, Z.P. Wei, X.H. Wang, C.X. Cong, Y.P. Xie, Y.M. Lu, D.Z. Shen, J. Lumin. 122–123 (2007) 191–194.